



1 **Temporal variability of tropospheric ozone and ozone**
2 **profiles in Korean Peninsula during the East Asian**
3 **summer monsoon: Insights from multiple**
4 **measurements and reanalysis datasets**

5

6

Juseon Bak^{1,*}, juseonbak@pusan.ac.kr

7

Eun-Ji Song^{1,a}, eunji@pusan.ac.kr

8

Hyo-Jung Lee¹, hyojung@pusan.ac.kr

9

Xiong Liu², xliu@cfa.harvard.edu

10

Ja-Ho Koo³, zach45@yonsei.ac.kr

11

Joowan Kim⁴, joowan@kongju.ac.kr

12

Wonbae Jeon^{1,5}, [wbjeon@pusan.ac.kr](mailto:wbyeon@pusan.ac.kr)

13

Jae-Hwan Kim⁵, jaekim@pusan.ac.kr

14

Cheol-Hee Kim^{1,5,*}, chkim2@pusan.ac.kr

15

16

¹*Institute of Environmental Studies, Pusan National University, Busan, South Korea*

17

²*Smithsonian Astrophysical Observatory (SAO), Center for Astrophysics | Harvard & Smithsonian*

18

³*Department of Atmospheric Sciences, Yonsei University, Seoul, Republic of Korea*

19

⁴*Department of Atmospheric Sciences, Kongju National University, Kongju, South Korea*

20

⁵*Department of Atmospheric Sciences, Pusan National University, Busan, South Korea*

21

^a*Currently at Department of Environmental Atmospheric Sciences, Pukyong National University, Busan, South Korea*

22

23

24

*Corresponding Author**

25

26

27

28

29



30

Abstract

31 We investigate the temporal variations of the ground-level ozone and balloon-based ozone profiles at
32 Pohang (36.02°N, 129.23°E) in Korean Peninsula. Satellite measurements and chemical reanalysis products
33 are also intercompared to address their capability of providing a consistent information on the temporal and
34 vertical variability of atmospheric ozone. Sub-seasonal variations of the summertime lower tropospheric
35 ozone exhibit a bimodal pattern related to atmospheric weather patterns modulated by the East Asian
36 monsoon circulation. The peak ozone abundances occur during the pre-summer monsoon with enhanced
37 ozone formation due to favorable meteorological conditions (dry and sunny). Ozone concentrations reach
38 its minimum during the summer monsoon and then reemerges in autumn before the winter monsoon arrives.
39 Profile measurements indicates that ground-level ozone is vertically mixed up 400 hPa in summer while
40 the impact of the summer monsoon on ozone dilution is found up to 600 hPa. Compared to satellite
41 measurements, reanalysis products largely overestimate ozone abundances in both troposphere and
42 stratosphere and give inconsistent features of temporal variations. Nadir-viewing measurements from the
43 Ozone Monitoring Instrument (OMI) slightly underestimate the boundary layer ozone, but well represent
44 the bimodal peaks of ozone in the lower troposphere and the interannual changes of the lower tropospheric
45 ozone in August, with higher ozone concentrations during the strong El Niño events and the low ozone
46 concentrations in during the 2020 La Niña event.

47

48 1. Introduction

49 Ground-level ozone should be reduced due to its adverse effect as a key air pollutant and greenhouse
50 gas in the troposphere, whereas stratospheric ozone should be protected for life on the Earth due to its
51 essential role in shielding harmful ultraviolet (UV) rays from the sun. Ozone is not directly emitted to the
52 atmosphere, but formed through the photolysis of oxygen molecules (O₂) by strong UV strikes in the
53 stratosphere as well as the photochemical process in which the photolysis of nitrogen dioxide (NO₂) by the
54 lights below 420 nm yields ozone in the troposphere.

55 This photochemical production has been strongly affected by the human activities damaging the
56 protective layer of the stratosphere with the emission of ozone-depleting substances (e.g., CFCs, Halon,
57 HCFCs) as well as boosting the ground-level ozone pollution with the emission of ozone precursors (CO,
58 VOCs, NO_x). In addition, the formation and fate of atmospheric ozone is complicatedly interacted with
59 meteorology and climate variability (Jacob and Winner, 2009; Lu et al., 2019; Zhang and Wang, 2016),



60 making it difficult to evaluate impacts of the emission control measures on ozone levels (Dufour et al.,
61 2021). As well, the tropospheric ozone is strongly influenced by either downward transport of stratospheric
62 air masses or the horizontal transport of polluted air-masses (Langford et al., 2015; Walker et al., 2010).

63 A monsoon is a seasonal change in atmospheric circulation and precipitation, affecting transport, wet
64 deposition, and chemical reactions on ozone and its precursors. The regional seasonality of ozone as well
65 as the latitudinal differences in ozone seasonality were attributed to the Asian monsoon-driven atmospheric
66 circulation (Tanimoto et al., 2005; Worden et al., 2009). In particular, impacts of the East Asian summer
67 monsoon (EASM) on spatiotemporal variations of surface-layer ozone concentrations over China have been
68 comprehensively addressed. For example, Yin et al. (2019) characterized the geographical distribution of
69 ozone in China, with a bimodal structure of ozone with a summer trough in the southern China whereas a
70 unimodal cycle in the northern China. Shen et al., (2022) specified the source-receptor relationships of
71 ozone pollution over the central and eastern China, mainly modulated by the monsoon circulation. Korean
72 Peninsula is located in the easternmost part of the Asian continent adjacent to the West Pacific where more
73 than a half of the total rainfall amount is typically concentrated during a short rainy season called Jangma
74 in summer, largely controlled by the EASM (Ha et al., 2012). The interannual and regional variabilities of
75 monsoon rainfall patterns over Korean Peninsula have been continuously and extensively established (Choi
76 et al., 2020; Ha et al., 2012), but rarely connected to impacts on the chemical composition.

77 The main objective of this paper is to characterize the temporal variability of tropospheric ozone and
78 ozone profiles, by linking with the meteorological variability largely controlled by the EASM. Ground-
79 based and balloon-based observations are collected from the Pohang station (36.02°N, 129.23°E) as a
80 reference dataset. The ground measurements are used to interpret the sub-seasonal variability of surface
81 ozone, while the vertical seasonality of ozone is investigated from ozonesondes. This paper is a preliminary
82 activity of the Asian Summer Monsoon Chemical and Climate Impact Project (ACCLIP) campaign
83 (<https://www2.acom.ucar.edu/acclip>) to investigate the impact of the Asian Summer Monsoon on regional
84 and global chemistry. The ACCLIP campaign will operate two aircrafts during the period July to August
85 in 2022 to measure atmospheric compounds through entire troposphere to lower troposphere over East Asia
86 and the West Pacific. The second objective of this paper is to evaluate whether the chemical reanalysis data
87 and remote-sensing data could represent a consistent picture of the summer monsoon impact on ozone
88 profile distribution. This evaluation will give an insight on the data selection used to fill in
89 the spatiotemporal gaps of the ACCLIP measurements.



90 2. Data descriptions

91 2.1 In-situ measurements

92 Ozonesondes are balloon-borne instruments capable of measuring the vertical distribution
93 of atmospheric ozone from the surface to balloon burst, usually near 35 km. The electrochemical
94 concentration cell (ECC)-typed sensor is the most widely employed. ECC ozonesondes have an uncertainty
95 of 5 %–10 % and a precision of 3 %–5 % (Smit et al., 2007). In South Korea, only at the Pohang station
96 ECC sondes have been regularly launched every Wednesday in the afternoon (13:30-15:30 LT) since 1995.
97 Ozonesonde measurements are reported in units of partial pressure (mPa) with vertical resolution of about
98 100 m by the Korea Meteorological Administration (KMA). Bak et al. (2019) demonstrated that Pohang
99 ozonesondes measurements are a stable set of reference profiles for validating satellite products.

100 Surface in-situ measurements of O₃ and NO₂ are collected from air quality monitoring networks of the
101 National Institute of Environmental Research (NIER) (AirKorea, <http://www.airkorea.or.kr>). This network
102 measures hourly air pollutants (O₃, NO₂, CO, SO₂) mixing ratios through the chemiluminescence
103 technology (Kley and Mcfarland, 1980). The KMA operates automatic synoptic observation system (ASOS)
104 at 102 weather stations. The ASOS measurements are provided in five types of time scales (minutely, hourly,
105 daily, monthly, yearly) via the KMA Weather Data Service (<https://data.kma.go.kr/>). We used daily
106 averages of air temperature, relative humidity, solar irradiance, total precipitation, wind speed, and wind
107 direction.

108 2.2 Satellite measurements

109 Both OMI and MLS were launched on board of NASA's EOS-Aura spacecraft in July 2004 and
110 still functioning in measuring the Earth's atmospheric composition. The Aura satellite crosses the equator
111 at ~ 1:30 in the afternoon. OMI is a nadir-viewing imaging spectrometer capable of daily, global mapping
112 at relatively high spatial resolution of 13 km × 24-48 km (across × along track). MLS measures microwave
113 thermal emission from the limb of Earth's atmosphere. Compared to OMI, MLS makes measurements at a
114 good vertical resolution (~ 3 km) in the upper atmosphere, but at relatively coarse horizontal resolutions
115 (~165 km along the orbit track). The version 4.2 of the MLS standard ozone product is used in this study,
116 only for the recommended vertical range from 261 to 0.025 hPa (Schwartz et al., 2015). We used OMI
117 ozone profiles retrieved using the PROFOZ version 2 algorithm which is in preparation for reprocessing
118 OMI measurements to release a new version of the OMPROFOZ research product (Liu et al., 2010). This
119 retrieval algorithm consists of wavelength/radiometric calibrations and forward modeling simulations, with



120 an optimal estimation inversion where a priori knowledge is optimally combined with measurement
121 information to obtain a better estimate of the state (Rodgers, 2000). The measurement sensitivity inherently
122 decreases toward the surface, with the increasing dependence of retrievals on the a priori information (Bak
123 et al., 2013). OMI sensitivity is very low to surface ozone, with its maximum in the free troposphere (~500
124 hPa) (Shen et al., 2019).

125 **2.3 Reanalysis data**

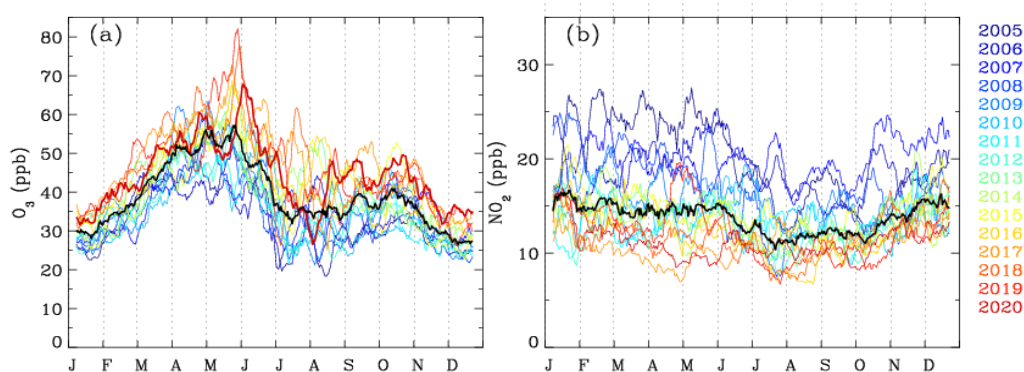
126 The Modern-Era Retrospective Analysis for Research and Applications, version 2 (MERRA-2), is
127 NASA's latest reanalysis, spanning the satellite observing era from 1980 to the present (Gelaro et al.,
128 2017). In addition to a standard meteorological analysis, a global O₃ field is driven by atmospheric
129 dynamics and constrained by satellite O₃ measurements using the GEOS-5 atmospheric model and the data
130 assimilation system. Beginning in October 2004, MERRA-2 assimilates total column ozone from OMI and
131 stratospheric ozone profiles above 215 hPa from MLS. Note that OMI total column ozone is assimilated to
132 account for the lower sensitivity of MLS measurements in the lower stratosphere, specifically in clouded
133 scenes.

134 The CAMS reanalysis is the latest global reanalysis data set of atmospheric composition produced by the
135 Copernicus Atmosphere Monitoring Service (CAMS), covering the period from 2003 to present (Inness et
136 al., 2019). Compared to MERRA-2, multiple satellite measurements were assimilated for the CAMS
137 reanalysis with ECMWF's Integrated Forecasting System. These included total ozone columns from
138 SCIAMARCY, OMI, and GOME/2 as well as ozone profiles from MIPAS and MLS after 2005.

139 Both reanalysis data have similar temporal and spatial resolutions. Merra-2 system produces 3-hourly
140 analyses at 72 sigma-pressure hybrid layers between the surface and 0.01 hPa, with a
141 horizontal resolution of $0.625^\circ \times 0.5^\circ$. The CAMS reanalysis data provide estimates every 3 hours with a
142 horizontal resolution of $0.75^\circ \times 0.75^\circ$. The vertical resolution of model consists of 60 hybrid sigma–pressure
143 (model) levels from surface to 0.1 hPa. In this study, we used CAMS global reanalysis (EAC4) monthly
144 averaged fields at 25 pressure levels (1000 hPa to 1 hPa) as well as MERRA-2 monthly mean data at 42
145 pressure levels (1000 hPa to 1 hPa). Both datasets provide ozone profiles in the unit of mixing ratio.

146 **3. Results and discussion**

147 **3.1. Temporal variability of ground-level ozone**



148

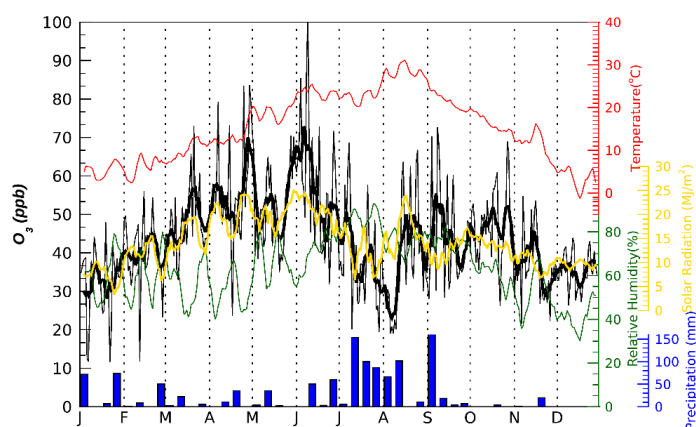
149 **Figure 1.** (a) Two-week moving averages of daytime ground-level ozone concentrations monitored at 6 sites in
150 Pohang, with (b) corresponding NO₂ concentrations. Different colorings represent each year from 2005 to 2020, while
151 the black line represents the mean ozone concentrations from all years.

152

153 Figure 1 shows both interannual and seasonal changes of daily ground-level concentrations of O₃
154 averaged at six AirKorea sites located within Pohang for 16 years (2005-2020) in comparison with its
155 primary precursor NO₂. Pohang is a major industrial city on South Korea's east coast, with the largest
156 population of North Gyeongsang Province. In this analysis, hourly measurements in afternoon (1-3 pm
157 local time) are first averaged for a given calendar day and then smoothed by two-week moving average.
158 The afternoon NO₂ do not change much seasonally. However, the seasonal cycle of ozone is bimodal with
159 peaks in early-summer and fall. Ozone concentration rapidly increases from ~ 30 ppb in January to primary
160 peak values of ~ 55 ppb on average during the period of late May to early June. The second peak of ozone
161 occurs in fall, which is much lower than the major peak.

162

163 In wintertime, the annual minimum of ozone concentrations gradually increases by ~ 10 ppb during
164 last 15 years whereas the annual maximum of summertime ozone rapidly increases from ~ 40 ppb to 80
165 ppb, in spite of the reduction of NO₂ amount by ~ 15 ppb or larger. Both depth and width of the summer
166 trough are highly variable, likely influenced by the strength and duration of the summer monsoon.



166

167 **Figure 2.** (Black) Daily ground-level ozone concentrations where weekly moving averages are applied (thick line) or
 168 not (thin line) at Pohang in 2020. The corresponding meteorological factors are overplotted; surface air temperature
 169 (red, °C), solar radiation (yellow, MJ/m²), and relative humidity (dark green, %). The bar graph shows the total
 170 precipitation (mm) for each week.

171 **Table 1.** Same as Figure2, but for correlation coefficients between ozone and meteorological variables, for pre-
 172 summer, summer, and post-summer periods, respectively.

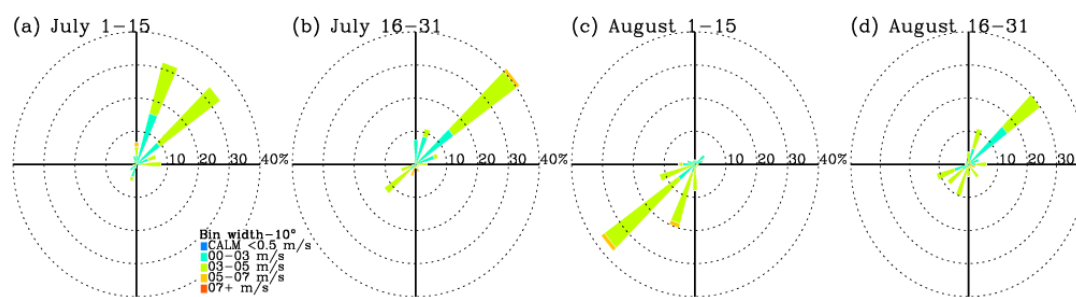
	pre-summer (Jan-May)	Summer (Jun-Aug)	Post-summer (Sep-Dec)
Solar radiation	0.91	0.74	0.51
Air temperature	0.79	-0.15	0.69
Relative humidity	-0.27	-0.64	0.59

173

174 In order to avoid smoothing out important features of intra-summer variations in ozone and their association
 175 with synoptic weather patterns, daily ozone and meteorological variables are zoomed in 2020 as one-week
 176 moving average (Figure 2). The local maximum of ozone concentrations is generally tied to the local warm,
 177 dry air and intense solar radiation before the rainy season starts. The correlation between ozone
 178 concentrations and meteorological variables is quantitatively compared in Table 1, for summer and
 179 post/pre-summer periods, respectively. Solar insolation amounts are directly linked to ozone concentrations
 180 over all seasons ($r=0.51-0.91$). The significant relationship between ozone and air temperature is also
 181 identified before and after summer seasons. However, in summer, ozone variations are rarely linked with
 182 temperature variations, due to the intense precipitation suppressing ozone formation. Consequently, the
 183 local minimum of ozone levels is tied to the local maximum of the relative humidity during the rainy season
 184 ($r=-0.64$). Note that the relative humidity is significantly influenced by air temperature, rather than amount



185 of water vapor in the pre and post summer periods. Therefore, in the post summer the correlation of ozone
186 with relative humidity ($r=0.59$) is likely to arise from the correlation of ozone with air temperature ($r=0.51$).
187 The rapid drop of ~ 10 ppb in ozone from the end of July to early August is hardly explained with
188 meteorological factors mentioned above; the weather becomes warmer with other meteorological variables
189 (precipitation and solar radiation) being relatively invariant. However, the prevailing wind is characterized
190 as southwesterlies in early August, exceptionally. Note that the northwesterly winds were dominant in July
191 and in late August (see. Figure 3). This summer minimum could deepen with the inflow of the poor
192 ozone airmass originated from the southern sea off the Korean peninsula into inland.



193

194 **Figure 3.** Wind roses for individual months from June through September in 2020 at Pohang. Note that hourly
195 observations in daytime are used to be consistent with data processing done in Figures 1 and 2.

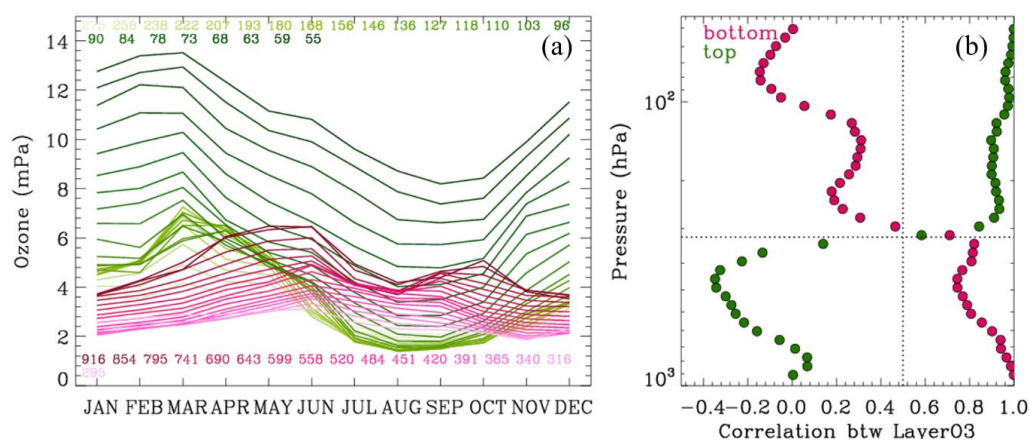
196

197 3.1. Temporal variability of ozone profiles

198 To understand the seasonality of ozone profiles, ozonesonde measurements collected at Pohang station
199 are climatologically averaged for each month and each pressure bin (~ 0.5 km intervals). Ozonesondes
200 soundings mainly measure ozone in the lower atmosphere below 10hPa while space-based limb soundings
201 mainly measure ozone in the upper atmosphere above 215hPa. However, both sounding measurements
202 provide the limited spatiotemporal information. OMI nadir measurements and reanalysis data provide the
203 daily global maps of ozone profiles. but the reliability of those data products should be assured before using
204 them to interpret ozone variability and its linkage to the monsoon circulation. As shown in Figure 4a, two
205 kinds of seasonal patterns are identified with a bimodal structure of layer ozone partial pressures in the
206 lower troposphere (LT) whereas a unimodal cycle in the upper troposphere and lower stratosphere (UTLS).
207 The LT ozone concentrations are peaked at June and October with a global minimum in winter as well as
208 a local summer minimum in late July and early August, which is consistent with surface measurements.



209 The concentrations of UTLS ozone are relatively higher in March due to the stratospheric intrusion, while
210 the minimum concentrations appear broadly over the summer and early fall due to the rise of the tropopause,
211 which is a common feature of ozone in the extratropical UTLS (Gettelman et al., 2011; Rao et al., 2003).
212 In order to quantify the similarity of seasonal variations, the correlation coefficient is calculated for
213 temporal ozone changes between each layer and the top/bottom layer. As shown in Fig. 4. b. the seasonality
214 of ozone at 50 hPa is significantly correlated down to ~ 300 hPa, with the correlation coefficient of larger
215 than 0.8. In addition, ozone in the boundary layer is significantly correlated with the lower tropospheric
216 ozone up to 700 hPa ($r > 0.9$) as well as the upper tropospheric ozone up to ~ 300 hPa ($r = 0.7-0.8$). It illustrates
217 that the 300 hPa could be regarded as a chemical barrier between troposphere and stratosphere at Pohang.



218

219 **Figure 4.** (a) Monthly variations of layer ozone partial pressures from ozonesonde soundings obtained from Pohang
220 during the period of 2005 to 2020. The legend values indicate the midpoint pressure of the layer (hPa). (b) Correlation
221 coefficients of monthly ozone variations between each layer and bottom layer (916 hPa in red)/top layer (55 hPa in
222 green).

223 In Figure 5, monthly averaged ozonesonde profiles are presented for 2020 and compared as a reference
224 to assess satellite measurements and reanalysis products. This contour map of ozonesondes clearly
225 illustrates the intrusion depth of the stratospheric air masses down to ~ 300 hPa during spring months (Fig
226 5a). The mixing depth of ozone that forms near the ground level is also identified, which is bounded up to
227 ~400 hPa in the summer and ~600 hPa in other seasons. The minimum ozone concentration is typically
228 found just below the thermal tropopause. The August minimum of the lower tropospheric ozone is vertically
229 extended above ~600 hPa. This air mass is much cleaner compared to the winter ozone concentration over
230 the lower troposphere. The dominant factor suppressing the ozone formation is a long-lasting summer
231 precipitation from early July to mid-Aug in 2020 (Fig.2). Southerly wind that blows on the observation site

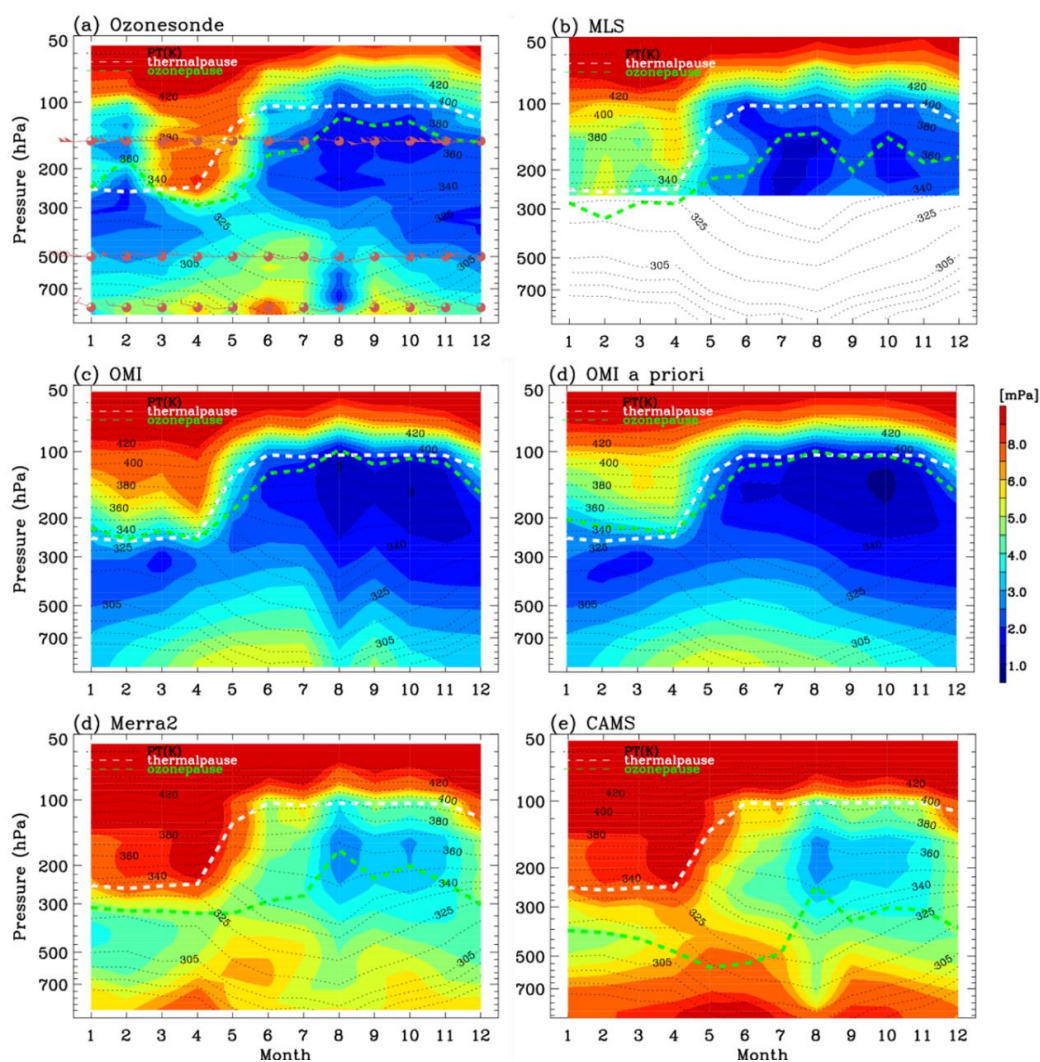


232 is relatively strong compared to June and July. Therefore, we could interpret that the inland polluted air
233 masses are likely to be diluted with the inflows of the maritime clean air masses as mentioned above. In the
234 lower troposphere, the minor peak of ozone concentrations is also identified in spring, which is not visible
235 in time-series plots of surface measurements (Fig. 2). The springtime peak is mainly originated by the fair
236 weather accelerating the formation of ground-level ozone with the wintertime accumulation of ozone and
237 its processors; it also could be partly attributed by the dynamical processes transporting the ozone-rich airs
238 from the UTLS and upwind areas. In Figures 5.b-f, OMI, MERRA-2, and CAMS ozone profiles are
239 qualitatively evaluated with respect to the capability of reproducing the seasonality of ozone profiles at
240 this location. The ozone minimum of summer monsoon season is detected from all ozone products, but
241 much broader than that in ozonesondes due to both the limited time resolution of ozonesonde measurements
242 and the limited spatial resolution of OMI and reanalysis products. OMI also show a very good agreement
243 with both ozonesonde in terms of reproducing the boundary layer ozone extending up to free troposphere
244 and low ozone concentration below the tropopause. In addition, the vertical gradient of ozone enhancement
245 above the tropopause is consistently reproduced from OMI, ozonesondes, and MLS. The spring ozone peak
246 near surface is not detectable from OMI measurements due to the limited sensitivity to relatively shallow
247 boundary layers compared to summer (Shen et al., 2019). In Figure 5.d, OMI a priori profile is also
248 presented to highlight that the summer minimum is derived from the independent information of OMI
249 measurements, rather than a priori information. It also illustrates that the summer minimum is a regional
250 feature of tropospheric ozone seasonality, not represented from the climatological data in which long-term
251 global measurements are composited as a function of month and latitude.

252 Both MERRA-2 and CAMS considerably overestimate ozone abundances in both troposphere and
253 stratosphere in spite of that MLS measurements are commonly employed for assimilating stratospheric
254 ozone profiles. In MERRA-2, the bimodal peaks (April and October) of the lower tropospheric ozone is
255 inconsistent with others (early summer, September). We also compare how each ozone product represents
256 the tropopause against thermally defined tropopause heights using the World Meteorological Organization
257 (WMO) definition (WMO, 1957). There is no universal method to define the ozonepause height, but
258 threshold values of 100 to 150 ppb in ozone mixing ratios were used to discriminate stratospheric to
259 tropospheric air masses (e.g., Hsu et al., 2005; Prather et al., 2011). In this paper, the 150 ppb value is
260 selected due to similarities of thermal tropopauses with ozone surfaces of 150 hPa from ozonesonde
261 measurements. As shown, the ozone surfaces at 150 ppb of reanalysis products are positioned in the free
262 troposphere due to the overestimation errors. Both ozonesonde and Aura measurements show somewhat



263 consistency between their ozone and thermal tropopause pressures. In particular, OMI shows the strong
264 consistency with the fact that retrievals near the tropopause are largely constrained with the a priori state
265 taken from the tropopause-based ozone profile climatology (Bak et al., 2013).



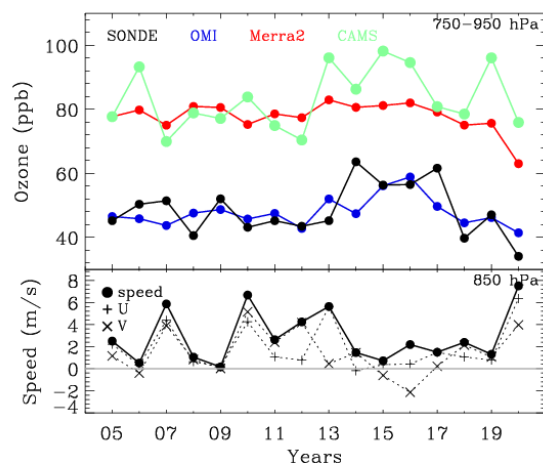
266
267 **Figure 5.** Contour plots of monthly ozone profiles in 2020 from (a) ozonesonde, (b) MLS, (c) OMI, (d) OMI a priori,
268 (e) MERRA-2, and (f) CAMS. The meteorological variables are superimposed for wind barbs (red symbols), potential
269 temperatures (black contours), thermal tropopause heights (white lines) using monthly MERRA-2 meteorological
270 data. The ozone value of 150 ppb is plotted with green lines for indicating the chemical transition between troposphere
271 and stratosphere.



272 **3.2. Interannual variability of lower tropospheric ozone in summer**

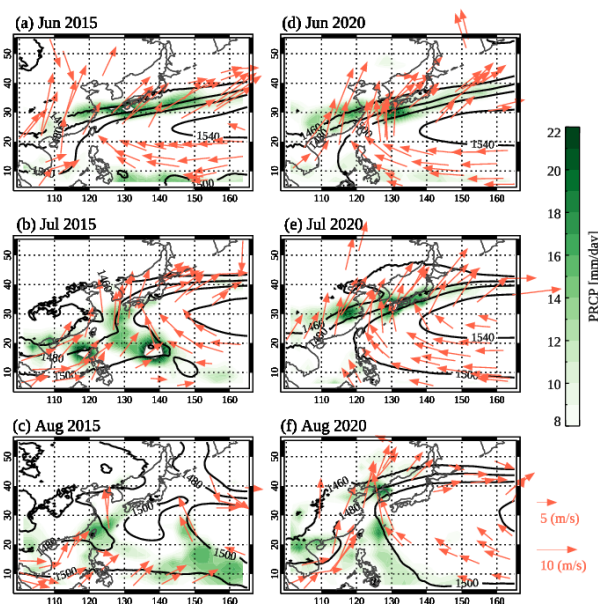
273 In this section, we focus on the ozone changes related to interannual meteorological variabilities, along
274 with the evaluation of different ozone products. In Figure 6, the time-series of mean ozone mixing ratio in
275 the lower troposphere (750-950 hPa) in August are compared. The summer monsoon typically ends in the
276 late July and early August over Korean peninsula and hence the ozone abundance in August is sensitive to
277 the intensity and duration of the monsoon season. OMI and ozonesonde show a similar long-term change,
278 except for much more fluctuations in time-series of ozonesondes due to insufficient samplings (weekly
279 observations) used in monthly averages. A noticeable correlation ($r = \sim -0.52$) exists between wind speeds
280 and ozone mixing ratios (ozonesonde). Low wind speed could enhance the accumulation of ozone
281 precursors and the rate of ozone formation. Accordingly, both ozonesonde and OMI measurements detect
282 higher ozone abundances in August from 2014 to 2017 when the wind speeds are relatively lower. As
283 shown in Figure 7 (a-c), where the monthly meteorological fields at 850 hPa in 2015 are presented from
284 MERRA-2 product, the western North Pacific Subtropical High (WNPSH) was broken in August and hence
285 the weather was likely to be calm and dry over the Korean peninsula. Compared to past few years, the lower
286 amount of ozone is detected in 2020 from ozonesonde measurements. In August 2020, the lower
287 tropospheric southwesterly winds blow from the western North Pacific to Korean Peninsula across the edge
288 of WNPSH as well as the rain belt over Korean Peninsula (Fig. 7. d-f). Therefore, the weather was windy
289 and wet, suppressing ozone formation in August 2020.

290 MERRA-2 ozone shows no annual variation, before 2020 unlike other ozone measurements and product.
291 CAMS also shows the higher ozone concentrations correlated with wind speeds, but less consistent with
292 ozonesonde measurements compared to OMI. How the El Niño-Southern Oscillation (ENSO) cycle
293 interacts with the East Asian monsoon has been not established. According to the Oceanic Niño Index, the
294 2015-2016 El Niño event, the warm phase of the ENSO, was one of the strongest events ever recorded,
295 whereas the 2020-2021 La Niña event was also abnormally strong. There was a lot of unprecedented
296 weather events in south Korea during these super El Niño and La Niña periods, such as
297 unprecedented summer rainfalls in 2020 and unprecedented summer heatwaves in 2015-2016 (Yoon et al.,
298 2018). Therefore, we could relate the higher ozone amount in August 2015-2017 and the lower ozone
299 amount in August 2020 to a climatic forcing on the strength and position of WNPSH and hence the East
300 Asian summer climate.



301

302 **Figure 6.** Annual variations of (top) the lower tropospheric ozone (750-950 hPa) in August from various ozone
 303 products, along with (bottom) the wind speeds at 850 hPa.



304

305 **Figure 7.** The monthly meteorological fields at 850 hPa for (a-c) 2015 and (d-f) 2020, respectively. The wind vectors
 306 are drawn with the orange arrows. The geopotential heights are superimposed with black lines. The variations of
 307 precipitation are shown with green typed colors, respectively. Note that we use MERRA-2 meteorological variables
 308 except for the precipitation data taken from GPCP Version 2.3 Combined Precipitation Data Set (Adler et al., 2003).

309



310 **4 Summary and Conclusions**

311 In this paper, atmospheric ozone variabilities over Korean peninsula and their linkages to the East
312 Asian summer monsoon are vertically characterized using multiple ozone measurements made by surface
313 observation, balloon-borne ozonesonde, OMI, and MLS. MERRA-2 and CAMS are also integrated in this
314 analysis for the evaluation against ozonesonde. Surface in-situ measurements at six urban sites in Pohang
315 are averaged, while satellite and reanalysis datasets are spatially interpolated onto the Pohang ozonesonde
316 site. Surface measurements clearly show the impact of frequent weather changes (dry and wet) on ozone
317 concentrations in spring. The seasonality of ozone becomes very complicated in late spring to early fall,
318 depending on monsoon strengths and lengths. The peak concentration of ozone occurs in the pre-summer
319 monsoon season (~ 70 ppb) and in the post-summer monsoon season (~50 ppb). During the summer
320 monsoon, ozone concentrations decrease down to ~ 30 ppb, which is even lower than that in the winter
321 when the air temperature and solar insolation is lowest. The vertical structures of ozone concentrations
322 driven by the stratospheric dynamics and synoptic scale tropospheric weather disturbances are
323 characterized from ozonesonde soundings. The stratospheric intrusions actively occur from March to May
324 and modulate the upper tropospheric ozone, down to ~ 300 hPa. We identified ozone enhancements in the
325 boundary layer, extending up to 400 hPa in June. In August the monsoon-induced ozone dilution occurs in
326 the lower troposphere up to ~ 600 hPa. The ozone minimum also occurs just below the tropopause, which
327 is deepest from summer to early fall with the troposphere being extending upward to ~ 100 hPa. Both
328 satellite and reanalysis datasets show the capability of reproducing general features of ozone seasonality
329 such as bimodal peaks in ground-level ozone and spring maximum in the UTLS ozone. However, MERRA-
330 2 and CAMS products significantly overestimates ozone abundances in the UTLS and hence middle
331 tropospheric ozone concentrations exceed 150 ppb which is used as a chemical proxy to distinguish between
332 stratospheric air and tropospheric air. In general, OMI shows a good agreement with ozonesonde
333 measurements with respect to both seasonal tendency and quantitative terms, but slightly underestimates
334 ground-level ozone due to the limited vertical sensitivity. The lower tropospheric ozone in August shows
335 the monsoon-induced interannual variabilities with higher concentrations during the super El Niño and
336 lower concentration during the significant La Niña period, commonly from ozonesonde and OMI
337 measurements. However, MERRA-2 rarely shows long-term changes of August ozone in the lower
338 troposphere. On the other hand, CAMS is annually correlated with ozonesonde measurements, but with the
339 systematic positive biases of ~ 40 ppb. In conclusion, OMI could play a vital role in studying the impact of
340 summer monsoon-derived atmospheric circulation and weather on ozone seasonality. The analysis results



341 of this study could be a useful reference to the upcoming results from the ACCLIP campaign planned in
342 the summer of 2022 to gather comprehensive, integrated datasets of two airborne observations (Flight
343 Operations from S. Korea) and ground/balloon measurements, over the East Asia and Western Pacific.
344 ACCLIP measurements will provide useful ideas for better understanding the spatiotemporal variation of
345 ozone in the Korean peninsula in terms of continuous ozone increase near the surface (Yoo et al., 2015),
346 high ozone in the free troposphere (Crawford et al., 2021), and the relationship between the stratospheric
347 ozone intrusion and atmospheric circulation (Park et al., 2012).

348

349 **Author Contributions** J.B and C.K designed the research; E.S interpreted the reanalysis products
350 and H.L and W.J contributed on analyzing surface measurements. X.L contributed on OMI ozone profile
351 retrievals. C.K and J.A.K provided oversight and guidance for connecting the weather condition and air
352 pollutant concentrations. J.K and J.O.K contributed to the interpretation of the results. J.B lead the writing
353 of the manuscript; all co-authors contributed to discussion and edited the paper.

354 **Competing interests.** The authors have no competing interests

355 **Acknowledgement**

356 We thank the KMA, NIER, NASA, and Copernicus for providing their measurements and analysis data.
357 We hope that the 2022 ACCLIP campaign could successfully be processed in South Korea and the research
358 outcome would be fascinating. We would like to acknowledge the Basic Science Research Program
359 (2020R1A6A1A03044834 and 2021R1A2C1004984).

360 *Financial support.* This research has been supported by the Basic Science Research Program through the
361 National Research Foundation of Korea (NRF) funded by the Ministry of Education (grant
362 no. 2020R1A6A1A03044834 and 2021R1A2C1004984)

363 **Data Availability**

364 Ozonesonde: <https://data.kma.go.kr> (last access: 16 Jun 2022)
365 AirKorea: <http://www.airkorea.or.kr> (last access: 16 Jun 2022)
366 ASOS: <https://data.kma.go.kr> (last access: 16 Jun 2022)
367 OMI ozone profile retrievals: attainable upon request (juseonbak@pusan.ac.kr)
368 MLS Version 4.2 ozone profile: <https://earthdata.nasa.gov> (last access: 16 Jun 2022).
369 MERRA-2 reanalysis data: <https://gmao.gsfc.nasa.gov/reanalysis/MERRA-2/> (last access: 16 Jun 2022).
370 CAMS global reanalysis (EAC4): <https://ads.atmosphere.copernicus.eu/> (last access: 16 Jun 2022).



371 GPCP Version 2.3 Combined Precipitation Data Set: <https://psl.noaa.gov/> (last access:16 Jun 2022)
372

373 References

374

- 375 Bak, J., Liu, X., Wei, J. C., Pan, L. L., Chance, K. and Kim, J. H.: Improvement of omi ozone profile
376 retrievals in the upper troposphere and lower stratosphere by the use of a tropopause-based ozone
377 profile climatology, *Atmos. Meas. Tech.*, 6(9), 2239–2254, doi:10.5194/amt-6-2239-2013, 2013.
- 378 Bak, J., Baek, K. H., Kim, J. H., Liu, X., Kim, J. and Chance, K.: Cross-evaluation of GEMS tropospheric
379 ozone retrieval performance using OMI data and the use of an ozonesonde dataset over East Asia
380 for validation, *Atmos. Meas. Tech.*, 12(9), 5201–5215, doi:10.5194/amt-12-5201-2019, 2019.
- 381 Bethan, S., Vaughan, G. and Reid, S. J.: A comparison of ozone and thermal tropopause heights and the
382 impact of tropopause definition on quantifying the ozone content of the troposphere, *Q. J. R.
383 Meteorol. Soc.*, 122(532), 929–944, doi:<https://doi.org/10.1002/qj.49712253207>, 1996.
- 384 Choi, J.-W., Kim, H.-D. and Wang, B.: Interdecadal variation of Changma (Korean summer monsoon
385 rainy season) retreat date in Korea, *Int. J. Climatol.*, 40(3), 1348–1360,
386 doi:<https://doi.org/10.1002/joc.6272>, 2020.
- 387 Crawford, J. H., Ahn, J.-Y., Al-Saadi, J., Chang, L., Emmons, L. K., Kim, J., Lee, G., Park, J.-H., Park,
388 R. J., Woo, J. H., Song, C.-K., Hong, J.-H., Hong, Y.-D., Lefer, B. L., Lee, M., Lee, T., Kim, S.,
389 Min, K.-E., Yum, S. S., Shin, H. J., Kim, Y.-W., Choi, J.-S., Park, J.-S., Szykman, J. J., Long, R.
390 W., Jordan, C. E., Simpson, I. J., Fried, A., Dibb, J. E., Cho, S. and Kim, Y. P.: The Korea–United
391 States Air Quality (KORUS-AQ) field study, *Elem. Sci. Anthr.*, 9(1),
392 doi:10.1525/elementa.2020.00163, 2021.
- 393 Dufour, G., Hauglustaine, D., Zhang, Y., Eremenko, M., Cohen, Y., Gaudel, A., Siour, G., Lachatre, M.,
394 Bense, A., Bessagnet, B., Cuesta, J., Ziemke, J., Thouret, V. and Zheng, B.: Recent ozone trends in
395 the Chinese free troposphere: role of the local emission reductions and meteorology, *Atmos. Chem.
396 Phys.*, 21(20), 16001–16025, doi:10.5194/acp-21-16001-2021, 2021.
- 397 Gelaro, R., McCarty, W., Suárez, M. J., Todling, R., Molod, A., Takacs, L., Randles, C., Darmenov, A.,
398 Bosilovich, M. G., Reichle, R., Wargan, K., Coy, L., Cullather, R., Draper, C., Akella, S., Buchard,
399 V., Conaty, A., da Silva, A., Gu, W., Kim, G.-K., Koster, R., Lucchesi, R., Merkova, D., Nielsen, J.
400 E., Partyka, G., Pawson, S., Putman, W., Rienecker, M., Schubert, S. D., Sienkiewicz, M. and
401 Zhao, B.: The Modern-Era Retrospective Analysis for Research and Applications, Version 2
402 (MERRA-2), *J. Clim.*, Volume 30(Iss 13), 5419–5454, doi:10.1175/JCLI-D-16-0758.1, 2017.
- 403 Gettelman, A., Hoor, P., Pan, L. L., Randel, W. J., Hegglin, M. I. and Birner, T.: THE
404 EXTRATROPICAL UPPER TROPOSPHERE AND LOWER STRATOSPHERE, *Rev. Geophys.*,
405 49(3), doi:<https://doi.org/10.1029/2011RG000355>, 2011.
- 406 Ha, K.-J., Heo, K.-Y., Lee, S.-S., Yun, K.-S. and Jhun, J.-G.: Variability in the East Asian Monsoon: a
407 review, *Meteorol. Appl.*, 19(2), 200–215, doi:<https://doi.org/10.1002/met.1320>, 2012a.
- 408 Ha, K.-J., Heo, K.-Y., Lee, S.-S., Yun, K.-S. and Jhun, J.-G.: Variability in the East Asian Monsoon: a
409 review, *Meteorol. Appl.*, 19(2), 200–215, doi:<https://doi.org/10.1002/met.1320>, 2012b.
- 410 Hsu, J., Prather, M. J. and Wild, O.: Diagnosing the stratosphere-to-troposphere flux of ozone in a
411 chemistry transport model, *J. Geophys. Res. Atmos.*, 110(D19),
412 doi:<https://doi.org/10.1029/2005JD006045>, 2005.
- 413 Inness, A., Ades, M., Agustí-Panareda, A., Barré, J., Benedictow, A., Blechschmidt, A.-M.,
414 Dominguez, J. J., Engelen, R., Eskes, H., Flemming, J., Huijnen, V., Jones, L., Kipling, Z.,
415 Massart, S., Parrington, M., Peuch, V.-H., Razinger, M., Remy, S., Schulz, M. and Suttie, M.: The
416 CAMS reanalysis of atmospheric composition, *Atmos. Chem. Phys.*, 19(6), 3515–3556,



- 417 doi:10.5194/acp-19-3515-2019, 2019.
- 418 Jacob, D. J. and Winner, D. A.: Effect of climate change on air quality, *Atmos. Environ.*, 43(1), 51–63,
419 doi:<https://doi.org/10.1016/j.atmosenv.2008.09.051>, 2009.
- 420 Langford, A. O., Senff, C. J., Alvarez, R. J., Brioude, J., Cooper, O. R., Holloway, J. S., Lin, M. Y.,
421 Marchbanks, R. D., Pierce, R. B., Sandberg, S. P., Weickmann, A. M. and Williams, E. J.: An
422 overview of the 2013 Las Vegas Ozone Study (LVOS): Impact of stratospheric intrusions and long-
423 range transport on surface air quality, *Atmos. Environ.*, 109, 305–322,
424 doi:<https://doi.org/10.1016/j.atmosenv.2014.08.040>, 2015.
- 425 Liu, X., Bhartia, P. K., Chance, K., Spurr, R. J. D. and Kurosu, T. P.: Ozone profile retrievals from the
426 Ozone Monitoring Instrument, *Atmos. Chem. Phys.*, 10(5), 2521–2537, doi:10.5194/acp-10-2521-
427 2010, 2010.
- 428 Lu, X., Zhang, L. and Shen, L.: Meteorology and Climate Influences on Tropospheric Ozone: a Review
429 of Natural Sources, Chemistry, and Transport Patterns, *Curr. Pollut. Reports*, 5(4), 238–260,
430 doi:10.1007/s40726-019-00118-3, 2019.
- 431 McPeters, R. D., Labow, G. J. and Logan, J. A.: Ozone climatological profiles for satellite retrieval
432 algorithms, *J. Geophys. Res.*, 112(D5), D05308, doi:10.1029/2005JD006823, 2007.
- 433 Park, S. S., Kim, J., Cho, H. K., Lee, H., Lee, Y. and Miyagawa, K.: Sudden increase in the total ozone
434 density due to secondary ozone peaks and its effect on total ozone trends over Korea, *Atmos.*
435 *Environ.*, 47, 226–235, doi:<https://doi.org/10.1016/j.atmosenv.2011.11.011>, 2012.
- 436 Prather, M. J., Zhu, X., Tang, Q., Hsu, J. and Neu, J. L.: An atmospheric chemist in search of the
437 tropopause, *J. Geophys. Res. Atmos.*, 116(D4), doi:<https://doi.org/10.1029/2010JD014939>, 2011.
- 438 Rao, T. N., Kirkwood, S., Arvelius, J., von der Gathen, P. and Kivi, R.: Climatology of UTLS ozone and
439 the ratio of ozone and potential vorticity over northern Europe, *J. Geophys. Res. Atmos.*, 108(D22),
440 doi:<https://doi.org/10.1029/2003JD003860>, 2003.
- 441 Rodgers, C. D.: *Inverse Methods for Atmospheric Sounding*, WORLD SCIENTIFIC., 2000.
- 442 Shen, L., Jacob, D. J., Liu, X., Huang, G., Li, K., Liao, H. and Wang, T.: An evaluation of the ability of
443 the Ozone Monitoring Instrument (OMI) to observe boundary layer ozone pollution across China:
444 application to 2005–2017 ozone trends, *Atmos. Chem. Phys.*, 19(9), 6551–6560, doi:10.5194/acp-
445 19-6551-2019, 2019.
- 446 Shen, L., Liu, J., Zhao, T., Xu, X., Han, H., Wang, H. and Shu, Z.: Atmospheric transport drives regional
447 interactions of ozone pollution in China, *Sci. Total Environ.*, 830, 154634,
448 doi:<https://doi.org/10.1016/j.scitotenv.2022.154634>, 2022.
- 449 Smit, H., Straeter, W., Johnson, B. J. J., Oltmans, S. J., Davies, J., Tarasick, D. W., Hoegger, B., Stübi,
450 R., Schmidlin, F. J., Northam, T., Thompson, A. M., Witte, J. C., Boyd, I. and Posny, F.:
451 Assessment of the performance of ECC-ozone sondes under quasi-flight conditions in the
452 environmental simulation chamber: Insights from the Juelich Ozone Sonde Intercomparison
453 Experiment (JOSIE), *J. Geophys. Res.*, 112, 2007.
- 454 Tanimoto, H., Sawa, Y., Matsueda, H., Uno, I., Ohara, T., Yamaji, K., Kurokawa, J. and Yonemura, S.:
455 Significant latitudinal gradient in the surface ozone spring maximum over East Asia, *Geophys. Res.*
456 *Letts.*, 32(21), doi:<https://doi.org/10.1029/2005GL023514>, 2005.
- 457 Walker, T. W., Martin, R. V., Van Donkelaar, A., Leaitch, W. R., MacDonald, A. M., Anlauf, K. G.,
458 Cohen, R. C., Bertram, T. H., Huey, L. G., Avery, M. A., Weinheimer, A. J., Flocke, F. M.,
459 Tarasick, D. W., Thompson, A. M., Streets, D. G. and Liu, X.: Trans-pacific transport of reactive
460 nitrogen and ozone to Canada during spring, *Atmos. Chem. Phys.*, 10(17), 8353–8372,
461 doi:10.5194/acp-10-8353-2010, 2010.
- 462 Worden, J., Jones, D. B. A., Liu, J., Parrington, M., Bowman, K., Stajner, I., Beer, R., Jiang, J., Thouret,
463 V., Kulawik, S., Li, J.-L. F., Verma, S. and Worden, H.: Observed vertical distribution of



- 464 tropospheric ozone during the Asian summertime monsoon, *J. Geophys. Res. Atmos.*, 114(D13),
465 doi:<https://doi.org/10.1029/2008JD010560>, 2009.
- 466 Yin, C. Q., Solmon, F., Deng, X. J., Zou, Y., Deng, T., Wang, N., Li, F., Mai, B. R. and Liu, L.:
467 Geographical distribution of ozone seasonality over China, *Sci. Total Environ.*, 689, 625–633,
468 doi:<https://doi.org/10.1016/j.scitotenv.2019.06.460>, 2019.
- 469 Yoo, J.-M., Jeong, M.-J., Kim, D., Stockwell, W. R., Yang, J.-H., Shin, H.-W., Lee, M.-I., Song, C.-K.
470 and Lee, S.-D.: Spatiotemporal variations of air pollutants (O_3 , NO_2 , SO_2 , CO,
471 PM_{10} , and VOCs) with land-use types, *Atmos. Chem. Phys.*, 15(18), 10857–10885,
472 doi:10.5194/acp-15-10857-2015, 2015.
- 473 Yoon, D., Cha, D.-H., Lee, G., Park, C., Lee, M.-I. and Min, K.-H.: Impacts of Synoptic and Local
474 Factors on Heat Wave Events Over Southeastern Region of Korea in 2015, *J. Geophys. Res.*
475 *Atmos.*, 123(21), 12,12-81,96, doi:<https://doi.org/10.1029/2018JD029247>, 2018.
- 476 Zhang, Y. and Wang, Y.: Climate-driven ground-level ozone extreme in the fall over the Southeast
477 United States, *Proc. Natl. Acad. Sci.*, 113(36), 10025–10030, doi:10.1073/pnas.1602563113, 2016.
478
- 479 Schwartz, M., Froidevaux, L., Livesey, N. and Read, W. (2015), MLS/Aura Level 2 Ozone (O_3) Mixing
480 Ratio V004, Greenbelt, MD, USA, Goddard Earth Sciences Data and Information Services Center
481 (GES DISC), Accessed: [Data Access Date], 10.5067/Aura/MLS/DATA2017
- 482 Adler, R.F., G.J. Huffman, A. Chang, R. Ferraro, P. Xie, J. Janowiak, B. Rudolf, U. Schneider, S. Curtis,
483 D. Bolvin, A. Gruber, J. Susskind, and P. Arkin: The Version 2 Global Precipitation Climatology
484 Project (GPCP) Monthly Precipitation Analysis (1979–Present). *J. Hydrometeor.*, 4,1147-1167,
485 2003
486